INTERNATIONAL JOURNAL FOR NUMERICAL METHODS IN FLUIDS
Int. J. Numer. Meth. Fluids 2007; **55**:655–672
Published online 5 April 2007 in Wiley InterScience (www.interscience.wiley.com). DOI: 10.1002/fld.1488

Modelling the effects of emergent vegetation on an open-channel flow using a lattice model

Francisco J. Jiménez-Hornero[1,*,†], Juan V. Giráldez[1], Ana M. Laguna[2], Sean J. Bennett[3] and Carlos V. Alonso[4]

[1]*Department of Agronomy, Hydraulic Engineering Section, University of Cordoba, Cordoba, Spain*
[2]*Department of Applied Physics, University of Cordoba, Cordoba, Spain*
[3]*Department of Geography, University at Buffalo, State University of New York, Buffalo, NY, U.S.A.*
[4]*National Sedimentation Laboratory, ARS, USDA, Oxford, MS, U.S.A.*

SUMMARY

A two-dimensional lattice model has been developed to describe the influence of vegetation on the turbulent flow structure in an open channel. The model includes the influence of vegetation density on the frictional effect of the channel bed and walls. For the walls, a semi-slip boundary condition has been considered as an alternative to overcome the no-slip boundary condition limitations in turbulent flows. The drag stress exerted by the flow on the vegetation as well as the gravity effect has also been taken into account. The proposed lattice model has been used to simulate the experimental results reported from the study of the influence of alternate vegetated zones on the open-channel flow. The results show that the lattice model approach is a valid tool for describing these kinds of flows. Copyright © 2007 John Wiley & Sons, Ltd.

Received 25 May 2006; Accepted 17 February 2007

KEY WORDS: lattice model; turbulence; vegetated flow; open channel

1. INTRODUCTION

Interest in using riparian vegetation in river restoration techniques has grown considerably in the last decade [1, 2]. Many field and laboratory experiments have been devoted to describing the interactions between flow, sediment transport and riparian vegetation. The effect of the emergent or submerged and rigid or flexible vegetation on the flow velocity and turbulent structure has been analysed in several works [3–13]. The drag coefficient of vegetation has been explored during the

*Correspondence to: Francisco J. Jiménez-Hornero, Albert Einstein (C2) Building, Campus Rabanales, University of Cordoba, Cordoba 14071, Spain.
†E-mail: ir2jihof@uco.es

Contract/grant sponsor: Spanish Ministry of Education and Research (MEC); contract/grant numbers: AGL2005-05326/AGR, AGL2006-10927-C03-03/AGR

last years [14–18]. The sediment transport in vegetated channels [19] and the efficiency of the vegetation trapping and sorting sediments [20] have also been described and measured.

The experiments on vegetated open channels [10] have shown that: (i) Flow velocities and near-bed shear stresses are reduced within vegetation zones. (ii) Turbulence intensity is increased near the canopy tops for submerged vegetation and along the interface between emergent riparian vegetation and the main channel. (iii) Vegetation increases local and boundary flow resistance. (iv) Vegetation reduces the flow transport capacity and causes sorting and deposition of sediment. (v) Vegetation creates secondary circulation patterns.

These complex phenomena have been simulated with different models. Among others, a depth-averaged two-dimensional k–ε model [21, 22] was proposed for describing the flow in vegetated open channels, combining it with a sediment transport model. Two-dimensional models [6] were used to characterize turbulent flow with vegetation effect. A large eddy simulation (LES) model [23] was developed to simulate the hydrodynamic behaviour of the turbulent flow in an open channel with a domain of vegetation. A Reynolds stress model [24] was applied to open-channel flows with vegetation. Two different turbulence closure schemes [25], a modified k–ε model and a two-layer model based on the mixing length approach, were used to study vegetation effects on the mean and turbulent flow structure.

Although the above-mentioned models are powerful tools, it is also of great interest to check the possibilities offered by other approaches with the aim of complementing the existing frameworks developed to simulate the complex effects of vegetation on the open-channel flow. The lattice model approach [26] is a particle-based numerical tool developed to simulate fluid dynamics. A lattice model is a synthetic physical system, whose microscopic rules are easy to simulate on a computer. Therefore, lattice models can be naturally applied to the description of complex phenomena. In addition, the lattice model simplicity, flexibility, intrinsic parallelism and the use of simple and regular meshes are features that permit this approach to be an alternative for solving partial differential equations [27].

The main aim of this work is to apply the lattice model framework for describing the interaction between vegetation and flow in an open channel. The model developed here simulates the turbulent flow using the LES technique and takes into account the influence of vegetation density on the channel bed and wall frictional stresses, as well as the drag stress exerted by the stream on the vegetation and the gravity effect. The model is validated by comparing the numerical predictions with the experimental flow patterns [10] in the presence of alternate zones of emergent vegetation when considering different vegetation densities.

2. METHODS

2.1. Modelling approach

In the experiments reported by [10, 11], the flows were subcritical and they did not display any significant vertical acceleration (i.e. hydrostatic pressure over the water column). Under these circumstances, the turbulent flow can be conceptualized as a two-dimensional and uniform-depth domain in which the space-filtered Navier–Stokes (NS) equations can be applied by using LES. This version of the NS equations requires more computer power than the Reynolds equations, time-averaged NS equations with a model for the turbulence stress such as the k–ε model. However, the space-filtered NS equations provide a more accurate solution to the turbulent flow [28].

DOI: 10.1002/fld

For a turbulent flow in the presence of emergent vegetation, the space-filtered NS equations can be written as follows:

$$\nabla\widetilde{\mathbf{u}} = 0 \tag{1}$$

and

$$h\frac{\partial\widetilde{\mathbf{u}}}{\partial t} + h(\widetilde{\mathbf{u}}\nabla)\widetilde{\mathbf{u}} = h\widetilde{v}\nabla^2\widetilde{\mathbf{u}} - ghs_s - \frac{1}{\rho}[\boldsymbol{\tau}_b + \boldsymbol{\tau}_w + \mathbf{d}_f] \tag{2}$$

in which h is the spatially averaged flow depth, t is the time, $\widetilde{\mathbf{u}}$ is the space-filtered flow velocity, g is the acceleration of gravity, $\mathbf{s}_s$ is the spatially averaged fluid surface slope, $\widetilde{v}$ is the effective or space-filtered kinematic viscosity, ρ is the fluid density, $\boldsymbol{\tau}_b$ and $\boldsymbol{\tau}_w$ are, respectively, the bed and wall shear stresses due to friction, and $\mathbf{d}_f$ is the drag stress exerted on vegetation.

The present modelling study approximates the flow pattern governed by Equations (1) and (2) using the lattice model scheme [29, 30]. This method describes fluid dynamics phenomena on a mesoscopic scale between the microscopic and macroscopic ones. At this level, the flow domain is transformed into a regular lattice where fluid particles move and interact continuously with each other following simple rules, conserving mass and momentum in the process [31, 32]. The lattice model used in this work, known as the BGK scheme [33, 34], is based on a simplification of its ancestor, the lattice Boltzmann model, using the relaxation time parameter [35] proposed in the context of collisions of gas molecules.

2.1.1. The lattice BGK scheme. In the BGK model, the particles move in a regular lattice, in which each node is linked to its neighbours following a vicinity model that is chosen depending on the complexity of the phenomenon to be simulated. To calculate the fluid velocity field in two dimensions the vicinity model *d2q9* is frequently used [26]. Figure 1 shows that model, in which $d = 2$ means the number of dimensions and $q = 9$ denotes the number of particles considered, in this case eight moving particles and one at rest, respectively. In the same figure, the independent variable f_i varies continuously between 0 and 1 according to the Boltzmann molecular chaos hypothesis and represents the probability of finding a particle in a link i that

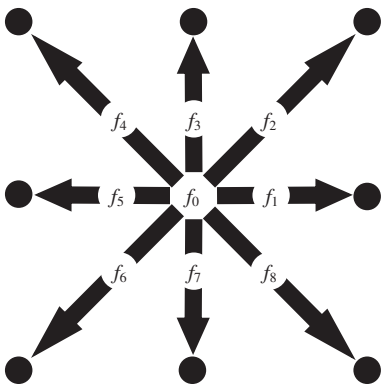

Figure 1. The vicinity model *d2q9* used in the simulations done with the proposed lattice BGK model; d and q denote the number of dimensions and particles (eight moving and one at rest), respectively.

DOI: 10.1002/fld

connects a node with one of its neighbours. The interactions of the particles keep up the mass and momentum [31, 32].

The equation of the lattice BGK model for a node $\mathbf{r}$ at time t, adopting the Einstein summation convention (i.e. repeated indices mean a summation over the space coordinates), is [26]

$$f_i(\mathbf{r}+\Delta t\mathbf{c}_i, t+\Delta t) = \frac{1}{\eta} f_i^{\mathrm{eq}}(\mathbf{r}, t) + \left(1-\frac{1}{\eta}\right) f_i(\mathbf{r}, t) + \frac{\Delta t}{c_\mathrm{s}^2} z_i c_{ik} F_k(\mathbf{r}, t) \tag{3}$$

where k represents the streamwise ($k=\alpha$) and lateral ($k=\beta$) directions, $\mathbf{c}_i$ is the velocity vector of a particle in the link i, which is defined by (4) considering $c=\Delta r/\Delta t$, with Δr being the length of the lattice spacing:

$$\mathbf{c}_i = \begin{cases} 0, & (i=0) \\ \alpha c \cos\left(\dfrac{\pi(i-1)}{4}\right) + \beta c \sin\left(\dfrac{\pi(i-1)}{4}\right), & (i=1,3,5,7) \\ \alpha\sqrt{2}c \cos\left(\dfrac{\pi(i-1)}{4}\right) + \beta\sqrt{2}c \sin\left(\dfrac{\pi(i-1)}{4}\right), & (i=2,4,6,8) \end{cases} \tag{4}$$

f_i^{eq} is the local equilibrium function, η is the relaxation time parameter that represents the difference between f_i and f_i^{eq}, z_i are weighting factors associated with the lattice directions, c_s is the speed of sound, a parameter selected according to the vicinity model chosen and F_k is the component of the external stress in the k direction. Using the Chapman–Enskog expansion, it is mathematically demonstrable that Equation (3) can recover the NS equations to the second order of accuracy [26, 29, 32] if f_i^{eq} is chosen in the following way:

$$\begin{aligned} f_i^{\mathrm{eq}} &= \rho z_i \left[1 + \frac{c_{ik}u_k}{c_\mathrm{s}^2} + \frac{1}{2}\left(\frac{c_{ik}u_k}{c_\mathrm{s}^2}\right)^2 - \frac{u_k u_k}{2c_\mathrm{s}^2}\right], \quad \forall i \in [1, q-1] \\ f_i^{\mathrm{eq}} &= \rho z_i \left(1 - \frac{u_k u_k}{2c_\mathrm{s}^2}\right), \quad i=0 \end{aligned} \tag{5}$$

For the *d2q9* neighbourhood model, it is found that $c_\mathrm{s}^2 = c^2/3$, $z_0 = \frac{4}{9}$, $z_{1,3,5,7} = \frac{1}{9}$ and $z_{2,4,6,8} = \frac{1}{36}$ [36].

The density ρ and velocity $\mathbf{u}$ are deduced from f_i according to

$$\begin{aligned} \rho(\mathbf{r}, t) &= \sum_{i=0}^{q-1} f_i(\mathbf{r}, t) \\ \mathbf{u}(\mathbf{r}, t) &= \frac{\sum_{i=1}^{q-1} f_i(\mathbf{r}, t)\mathbf{c}_i}{\rho(\mathbf{r}, t)} \end{aligned} \tag{6}$$

and the kinematic viscosity, υ, is defined as

$$\upsilon = \frac{\Delta r^2}{\Delta t} c_\mathrm{s}^2 \left(\eta - \frac{1}{2}\right) \tag{7}$$

DOI: 10.1002/fld

With the aim of simulating turbulent flows, the LES technique is adapted to the lattice BGK model in the way suggested by [37]. Thus, the effective viscosity $\widetilde{\upsilon}$, made up of the original kinematic viscosity υ and an eddy viscosity υ_t, is considered:

$$\widetilde{\upsilon} = \upsilon + \upsilon_t \tag{8}$$

The eddy viscosity has been determined in this work using the Smagorinsky eddy viscosity model [26, 38, 39], where υ_t is defined as

$$\upsilon_t = C_{\text{smago}}^2 \Delta^2 |S| \tag{9}$$

where Δ is the filter size, that usually corresponds to Δr. It is frequent to assume in the lattice BGK model simulations $\Delta r = \Delta\alpha = \Delta\beta = 1$ lattice unit and $\Delta t = 1$ time step [26]. Thus, $\Delta = 1$. The magnitude of the strain-rate tensor, $S_{\alpha\beta}$, is $|S| = \sqrt{2S_{\alpha\beta}S_{\alpha\beta}}$ and the external parameter C_{smago} is called the Smagorinsky constant. The spatially filtered relaxation time $\widetilde{\eta}$ is related to the original η and eddy η_t relaxation times from (9) as

$$\widetilde{\eta} = \frac{\widetilde{\upsilon}}{c_s^2} + \frac{1}{2} = \frac{\upsilon + \upsilon_t}{c_s^2} + \frac{1}{2} = \eta + \frac{\upsilon_t}{c_s^2} = \eta + \eta_t \tag{10}$$

The strain-rate tensor can be deduced from the non-equilibrium momentum flux tensor, $\Pi_{\alpha\beta}$, in the following way [32, 40]:

$$|S| = \frac{1}{2\rho(\eta + \eta_t)} \frac{1}{c_s^2} \sqrt{\Pi_{\alpha\beta}\Pi_{\alpha\beta}} \tag{11}$$

with

$$\Pi_{\alpha\beta} = \sum_i c_{i\alpha} c_{i\beta} (f_i - f_i^{\text{eq}}) \tag{12}$$

Once $|S|$ is calculated from (11) considering (12), its value is replaced in (9) and, considering (10), the expression for $\widetilde{\eta}$ can be obtained:

$$\widetilde{\eta} = \frac{1}{2} \left(\eta + \sqrt{\eta^2 + 2C_{\text{smago}}^2 \frac{\sqrt{\Pi_{\alpha\beta}\Pi_{\alpha\beta}}}{\rho}} \right) \tag{13}$$

The spatially filtered equation of the lattice BGK model is obtained by replacing η by $\widetilde{\eta}$ in (3) [26]:

$$f_i(\mathbf{r} + \mathbf{c}_i, t+1) = \frac{1}{\widetilde{\eta}} f_i^{\text{eq}}(\mathbf{r}, t) + \left(1 - \frac{1}{\widetilde{\eta}}\right) f_i(\mathbf{r}, t) + \frac{1}{c_s^2} z_i c_{ik} F_k(\mathbf{r}, t) \tag{14}$$

where $\Delta r = 1$ lattice unit and $\Delta t = 1$ time step. By using the f_i's derived from (14) and substituting them in (6), the spatially filtered velocity $\widetilde{\mathbf{u}}(\mathbf{r}, t)$ can be determined.

To simulate a turbulent flow with the lattice BGK and Smagorinsky models, it is necessary to fit empirically C_{smago} depending on the configuration of the flow. This is the main drawback of the use of the Smagorinsky subgrid scale model.

The conversion rules between the magnitudes used in the proposed lattice BGK model and their corresponding physical values [26] are shown in Table I. The scale factors Δr and Δt are,

DOI: 10.1002/fld

Table I. Conversion rules between the magnitudes used in the lattice BGK model and their physical values [26].

Magnitude	Lattice BGK model	Physical value
Time	t	$t^{\text{real}} = \Delta t\, t$
Space	r	$r^{\text{real}} = \Delta r\, r$
Velocity	u	$u^{\text{real}} = (\Delta r/\Delta t)u$
Acceleration of gravity	g	$g^{\text{real}} = (\Delta r/\Delta t^2)g$
Kinematic viscosity	υ	$\upsilon^{\text{real}} = (\Delta r^2/\Delta t)\upsilon$

Note: The scale factors Δr and Δt are expressed in SI units.

respectively, the length of the lattice spacing and the time elapsed during one iteration or time step expressed in SI units.

2.1.2. The external stress in the lattice BGK model. As shown in (14), the external stress can be included in an easy way in the lattice BGK model equation [40, 41]. In the model proposed here for flow in an open and vegetated straight channel, the external stress consists of the bed and wall shear stresses due to friction, $\boldsymbol{\tau}_{\text{b}}$ and $\boldsymbol{\tau}_{\text{w}}$, respectively, the drag stress exerted on vegetation, $\mathbf{d}_f$, and the effect of gravity, g, by considering the fluid surface slope, $\mathbf{s}_{\text{s}}$. For the spatial direction k, F can be expressed as

$$F_k(\mathbf{r}, t) = -g(1 - \chi_{\text{b}})s_{sk} - \frac{1}{h}[\tau_{\text{b}k}(\mathbf{r}, t) + \tau_{\text{w}k}(\mathbf{r}, t) + d_{fk}(\mathbf{r}, t)] \tag{15}$$

where $h = 1$ lattice unit is adopted, $g = 9.81\,\text{m}\,\text{s}^{-2}$ $(\Delta t^2/\Delta r)$ according to Table I and χ_{b} is the fraction of bed occupied by the vegetation in the zones where it is placed. For the vegetated area shown in Figure 2, $\chi_{\text{b}} = 2N\phi^2/\theta^2$, with N as the number of vegetation elements, ϕ as the diameter of each vegetation element and θ as the diameter of the semi-circular vegetated area. Otherwise, $\chi_{\text{b}} = 0$.

The shear stress due to bed friction is included in the lattice BGK model by means of the expression (16) derived from [42] taking into account χ_{b}:

$$\tau_{\text{b}k} = C_{\text{b}}(1 - \chi_{\text{b}})\widetilde{u}_k|\widetilde{u}| \tag{16}$$

C_{b} is a non-dimensional bed friction coefficient calculated from

$$C_{\text{b}} = \frac{gn_{\text{b}}^2}{h^{1/3}} \tag{17}$$

where n_{b} is the Manning roughness coefficient at the bed and h is expressed in SI units (i.e. the real value reported from the experiments).

In a similar way [43], the shear stress in the channel walls is considered as

$$\tau_{\text{w}k} = C_{\text{w}}(1 - \chi_{\text{w}})\widetilde{u}_k|\widetilde{u}| \tag{18}$$

where, C_{w} is a non-dimensional friction coefficient calculated from (17) replacing n_{b} by the Manning roughness coefficient at the walls, n_{w}. In this work $n_{\text{b}} = n_{\text{w}}$ is assumed. The fraction of the channel wall area, χ_{w}, covered by the vegetation elements is calculated from $\chi_{\text{w}} = \phi/b_{\text{v}}$ in the case of Figure 2, with b_{v} being the vegetation spacing. For non-vegetated areas, $\chi_{\text{w}} = 0$.

DOI: 10.1002/fld

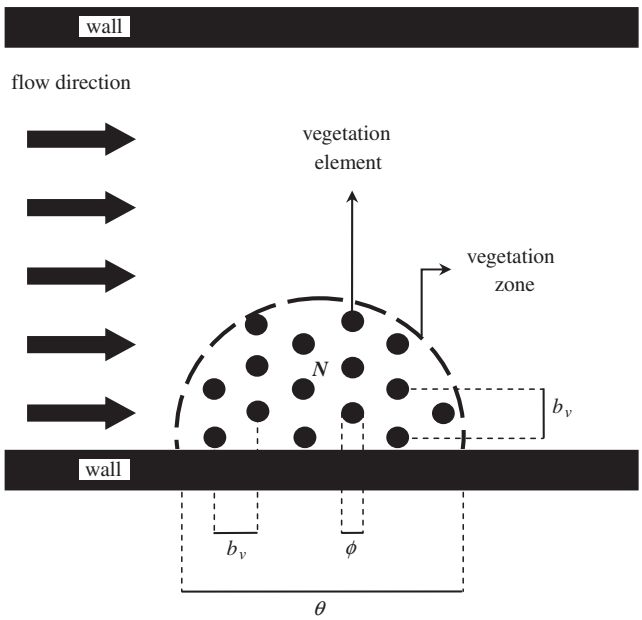

Figure 2. Scheme used in the computation of the projected area of the vegetation in the streamwise direction, A_v, according to expression (20). The vegetated zone (dashed line) is a semi-circle with a diameter θ containing N similar emergent vegetation elements (black dots) in a staggered arrangement with a diameter ϕ separated between them by a distance b_v. The sum of the projected areas of the vegetation elements in the streamwise direction is $A_{nv} = N\phi\mu h$, with μ being the shape factor of vegetation. The projected area of the vegetated zone in the same direction is $A_{vz} = h\theta/2$, with $A_v = 2N\phi\mu/\theta$.

Finally, the drag stress exerted by the flow on vegetation is [44]

$$d_{fk} = \tfrac{1}{2} C_d A_v \widetilde{u}_k |\widetilde{u}| \tag{19}$$

with C_d as a non-dimensional drag coefficient related to the flow and vegetation characteristics [45]. The parameter A_v represents the relationship between the area of the vegetation elements, A_{nv}, and the area of the vegetated zone where they are placed, A_{vz}, both projected in the streamwise direction so that

$$A_v = \frac{A_{nv}}{A_{vz}} \tag{20}$$

For the scheme shown in Figure 2, $A_{nv} = N\phi\mu h$, with μ being a non-dimensional shape factor of vegetation related to its irregularity and flexibility and $A_{vz} = h\theta/2$, resulting in $A_v = 2N\phi\mu/\theta$.

2.1.3. Boundary conditions. In all the lattice BGK model simulations carried out here, the flow is determined by assigning the spatially averaged velocity u_0 at the inlet of the computational domain and the periodic boundary condition is applied at the outlet.

Because of considering the shear stress in channel walls, the boundary condition applied at these places has to be different from the common bounce-back rule used in lattice BGK models for

DOI: 10.1002/fld

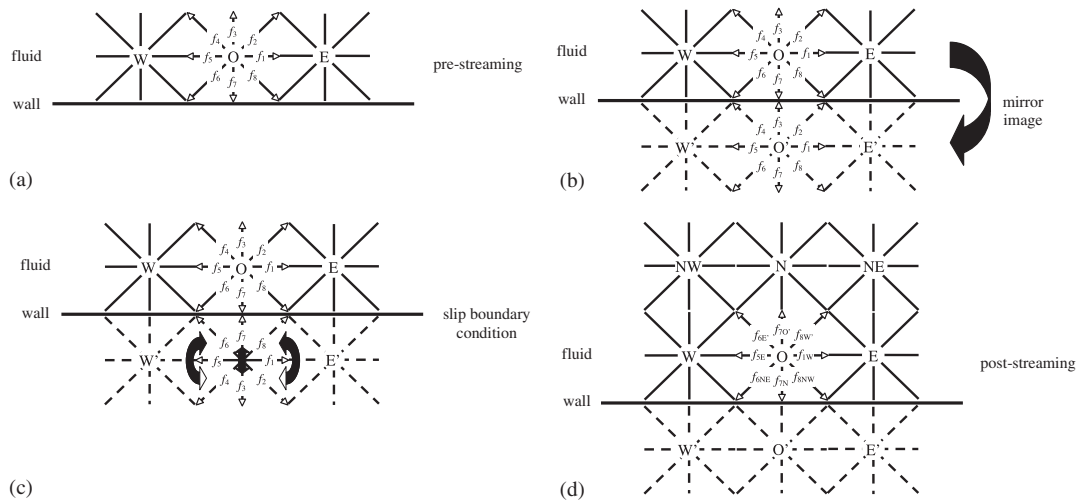

Figure 3. Diagram of the mirror-image method proposed by [46] for impermeable boundary treatment. It corresponds to the slip boundary condition that, combined with the channel wall shear stress, leads to the semi-slip boundary condition proposed by [43] for turbulent flows: (a) the distribution functions are calculated in O from (14); (b) application of the mirror-image method copying the f_i's of cell O in an imaginary cell O'; (c) slip boundary condition changing the adequate values of f_i's in O'; and (d) values of the f_i's in O' after the streaming step.

simulating solids. There is a large velocity gradient near a solid boundary for turbulent flows due to wall friction [43], which cannot be simulated correctly with a no-slip boundary condition. One alternative for dealing with these kinds of boundaries is the semi-slip boundary condition proposed by [43], which has been adopted here. It consists of a combination of the shear stress (18) with the slip boundary condition indicated in Figure 3 according to [46] at the places marked as channel wall in the computational domain. In the pre-streaming phase (Figure 3a), the so-called collision step, the value of f_i is calculated using (14) for each link i at node O. In order to apply the slip boundary condition, it is necessary to determine the missing distribution functions f_2, f_3 and f_4 that arise from cells outside the domain that are imaginary. Following [46], the distribution functions can be calculated from those corresponding to the cells inside the domain using the mirror-image method (Figure 3(b)). The slip boundary condition is applied at the imaginary cells (O', W' and E') changing the distribution functions in the way described in Figure 3(c). As a consequence, the sum of momentum normal to the wall is zero. The new values of f_i at O after the streaming step are shown in Figure 3(d). Using them in (14), it was possible to derive the velocity for calculating the wall shear stress from (18).

2.2. Laboratory experiments on the flow around alternate vegetation zones

The experiments on the flow in the presence of alternate emergent vegetation zones presented in [10] were conducted using a tilting re-circulating flume of $l = 16.5\,\mathrm{m}$ in length and $w = 0.6\,\mathrm{m}$ in width. Its scheme is shown in Figure 4. The flume was equipped with an upstream baffle to damp pump-related turbulence and a downstream weir to establish a uniform flow regime. The flow discharge P was kept constant at $0.0042\,\mathrm{m}^3\,\mathrm{s}^{-1}$ in all the experiments. Flow depths were

DOI: 10.1002/fld

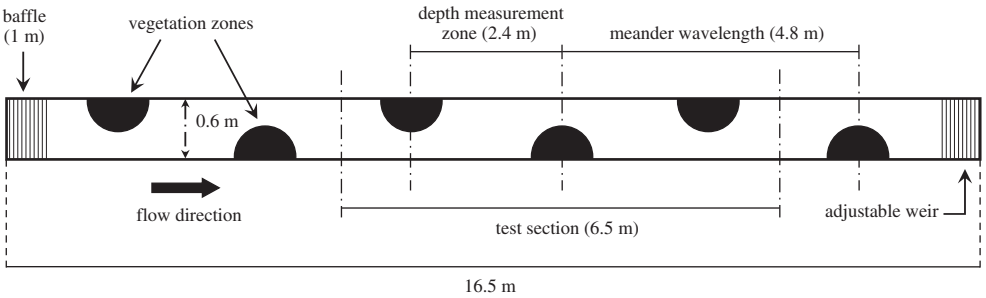

Figure 4. Diagram of the experimental channel used by [10] to study the turbulent flow structures caused by emergent vegetation placed in alternate zones.

Table II. Some relevant features of the experiments performed by [10] with two different vegetation densities, VD.

Vegetation zones		Averaged flow parameters				
Dowels per zone, N	Distance between rows and columns, b_v ($\times 10^{-3}$ m)	VD (m^{-1})	P ($m^3\,s^{-1}$)	h (m)	u_0 ($m\,s^{-1}$)	$s_{s\alpha}$ ($\times 10^{-3}$)
113	36	0.176	0.0042	0.026	0.267	−1.52
1753	9	2.739	0.0042	0.036	0.196	−1.95

Note: P is the flow discharge and h, u_0 and $s_{s\alpha}$ are the spatially averaged flow depth, velocity and water surface slope, respectively.

measured over a 2.4 m longitudinal section excluding the vegetation zones, and these data were used to calculate the spatially averaged flow depth h, velocity u_0 and water surface slope $s_{s\alpha}$.

A total of six alternate vegetation zones were placed along the length flume spaced at a distance $\lambda = 4.8$ m to each other, λ was the so-called meander wavelength (Figure 4). The shape of the vegetated areas was semi-circular with a diameter of $\theta = 0.6$ m. The emergent vegetation was simulated by using wooden dowels of $\phi = 3.2 \times 10^{-3}$ m in diameter and 70×10^{-3} m in height [10]. For a specific vegetation density VD, a number of dowels N were placed perpendicularly to the plywood flume floor in a staggered arrangement with spacing b_v to maximize the flow resistance (Figure 2). The definition of vegetation density (21), expressed in m^{-1} and adopted in the experiments, was the ratio between the sum of the frontal areas of the vegetation divided by the volume of fluid (depth water over an area encompassing one meander wavelength λ):

$$\mathrm{VD} = \frac{N\phi h}{w\lambda h} \tag{21}$$

Particle image velocimetry (PIV) was used to characterize the surface flow field for the test area marked in Figure 4 considering different vegetation densities. The experimental results obtained by [10] with VD = 0.176 and 2.739 m^{-1} in nine cross-sections were reported in [21]. Table II summarizes some relevant features of these experiments.

DOI: 10.1002/fld

3. RESULTS

3.1. Grid independence study

The data corresponding to the time-averaged velocity, u_m, when VD = 0 were collected across the experimental flume at three downstream different distances from the origin of the test section, 3.02 m (velocity profile 1), 5.02 m (velocity profile 2) and 6.94 m (velocity profile 3) and they were used to perform a grid independence study. Figure 5 shows these data, with y being the distance from the right flume wall. These velocity profiles were selected because they displayed the least spread. The momentum exchange vanishes across the flume plane of symmetry and, thus, this plane can be treated as the free surface of a virtual uniform flow of depth $0.5w$ in an infinitely wide channel. The velocity data set was interpreted as the equilibrium velocity distribution within the virtual uniform flow. The Kármán–Prandtl equation to compute the velocity defect with respect to the average velocity across the channel results in

$$u_m = a \log\left(\frac{y}{0.5w}\right) + b \tag{22}$$

with $a = 2\sqrt{8}u^*$ and $b = 0.88\sqrt{8}u^* + \overline{u}_\mathrm{p}$, where u^* is the shear velocity on the virtual channel bottom and $\overline{u}_\mathrm{p}$ is the average of the velocity profile across the flow depth.

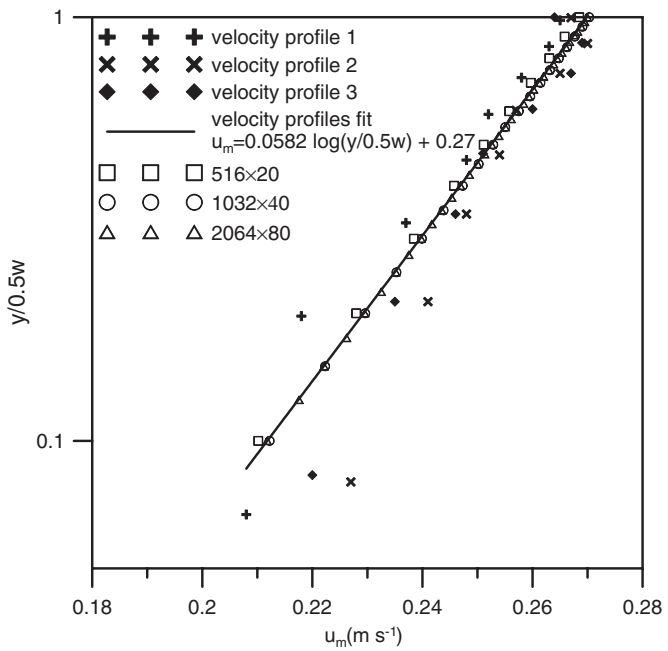

Figure 5. Grid independence study carried out considering three computational domain sizes of 516×20, 1032×40 and 2064×80 lattice units. The logarithmic law for turbulent flows, represented by the fit obtained for the experimental velocity profiles 1, 2 and 3, was acceptably reproduced in all the cases. The results obtained with the computational domain sizes of 1032×40 and 2064×80 lattice units are grid independent.

DOI: 10.1002/fld

The values of $a = 0.0582$ and $b = 0.27$ were obtained from the fit of (22), shown in Figure 5, to the experimental velocity profiles. The goodness of the fit, determined by using the Nash–Sutcliffe efficiency [47], $E \in (-\infty, 1]$, was $E = 0.9332$. Thus, $u^* = 0.0103\,\mathrm{m\,s^{-1}}$ and $\overline{u}_\mathrm{p} = 0.27\,\mathrm{m\,s^{-1}}$ were derived. The boundary roughness corresponding to this velocity profile was determined by using the Darcy–Weisbach resistance coefficient, fr, computed from the relation $u^* = \overline{u}_\mathrm{p}\sqrt{fr/8}$. The estimated value for fr was 0.01164. The expression for the Reynolds number of a flow of uniform depth $0.5w$ in an infinitely wide channel yields $Re = 4(0.5w)\overline{u}_\mathrm{p}/\upsilon = 3.24 \times 10^5$. Entering fr and Re in the Moody diagram modified for open-channel flows, it is seen that the flume wall behaves as a hydrodynamically smooth surface [48, Figure 2.5.1]. From these results, the following can be concluded: (i) the average velocity of the flow on the free-surface plane, $\overline{u}_\mathrm{p}$, is lower than the spatially averaged velocity, $u_0 = 0.307\,\mathrm{m\,s^{-1}}$ [10, 11]; (ii) the velocity distribution on the free-surface plane follows the logarithmic law for turbulent flows; and (iii) the flume wall behaves as a hydrodynamically smooth boundary in agreement with the conditions in the experiments.

A grid independence study was performed by considering three computational domains with sizes of 516×20 ($\Delta r = 0.03\,\mathrm{m}$, $\Delta t = 0.01\,\mathrm{s}$, $\eta = 0.500033$), 1032×40 ($\Delta r = 0.015\,\mathrm{m}$, $\Delta t = 0.005\,\mathrm{s}$, $\eta = 0.500066$) and 2064×80 ($\Delta r = 0.0075\,\mathrm{m}$, $\Delta t = 0.0025\,\mathrm{s}$, $\eta = 0.500133$), in lattice units. The value selected for C_smago was 0.12, frequently used by researchers [49]. The Smagorinsky model works well for channel flows with the value adopted for C_smago [50] because it reduces the energy dissipation near the walls. In all the cases, $s_{s\alpha} = -1.55 \times 10^{-3}$ [10] and the parameters C_b and C_w were calculated from (17) considering $n_\mathrm{b} = n_\mathrm{w} = 0.015\,\mathrm{m^{-1/3}\,s}$ and $h = 0.023\,\mathrm{m}$. The value of the Manning roughness coefficient was not reported by [10, 11]. The value adopted here for the flume plywood corresponds to that suggested by [51, Tables 5 and 6] for laminated wood. The velocity was set to $0.307\,\mathrm{m\,s^{-1}}$ at the inlet in all the tests. The time-averaged velocity profiles at 3.02, 5.02 and 6.94 m downstream distances from the origin of the test section were simulated for each computational domain size. Figure 5 shows the fits obtained for those velocity profiles that are not represented for the sake of clarity. It can be verified that the logarithmic law for turbulent flows was well reproduced in all the cases. However, the experimental velocity data fit was better matched when the size of the computational domain is 1032×40 ($E = 0.99911$) or 2064×80 ($E = 0.99957$) compared to the case of 516×20 ($E = 0.995$). This fact shows that the results obtained with the computational domain sizes of 1032×40 and 2064×80 lattice units are grid independent.

The simulations were run on a SGI Origin 2000 server with eight MIPS R10000 processors (200 MHz). However, only six processors were used in the calculations because two processors were always busy running tasks belonging to other users. A standard simulation consisted of 5×10^4 time steps and it took 300, 1200 and 4800 s for the computational domain sizes of 516×20, 1032×40 and 2064×80 lattice units, respectively. Therefore, adopting a compromise between the computational time and accuracy of the results, the domain of 1032×40 lattice units was selected to perform the simulations with the proposed lattice BGK model.

3.2. Simulation of the vegetation density influence on the turbulent flow structure

The values adopted for Δr, Δt, η, C_smago, n_b and n_w in the simulations were equal to those used in the grid independence study for the computational domain size of 1032×40 lattice units. For the vegetation densities simulated, the velocity was set to the corresponding values of u_0 listed in Table II at the inlet, while the periodic and semi-slip boundary conditions were applied

DOI: 10.1002/fld

Table III. Values of the parameters used in the lattice BGK model for the simulation of the experiment results described by [10] for two different vegetation densities, VD.

VD (m^{-1})	$C_b = C_w$	χ_b	χ_w	C_d	A_v
0.176	0.00744	0.00642	0.088	1.1	2.411
2.739	0.00709	0.09973	0.355	2.85	37.397

Note: C_b and C_w are the channel bed and walls friction coefficients. χ_b and χ_w represent the fractions of the channel bed and wall areas covered by the vegetation. C_d is a non-dimensional drag coefficient and A_v stands for the normalized area of the vegetation elements projected in the streamwise direction.

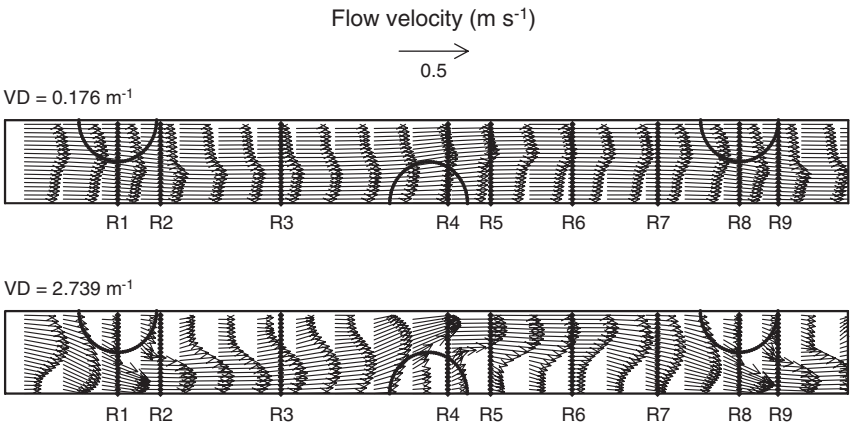

Figure 6. Time-averaged surface flow pattern simulated with the proposed lattice BGK model for the test section (Figure 4) of the experiment performed by [10] for two different vegetation densities (VD). The vegetation zones are represented by semi-circles. The vertical lines R_j, $j \in [1, 9]$, mark the places where the surface flow velocities were measured.

at the outlet and the flume walls, respectively. The values of h and $s_{s\alpha}$ used in the simulations are reported in Table II. Regarding the vegetated zones, χ_b, χ_w and A_v were deduced from the experimental arrangement of the simulated vegetation elements described by [10]. The shape factor for the rigid cylinders was assumed as $\mu = 1$. Table III summarizes the values of the parameters used to simulate the two vegetation densities considered. The drag coefficient, C_d, had to be obtained from calibration by comparing the simulated and measured surface flow velocities [10, 21] in the test sections marked in Figure 6 and shown in Figures 8 and 9. For VD = 0.176 and 2.739 m^{-1}, they were fitted to 1.1 and 2.85, respectively. These values were similar to those calibrated by [21], 1.2 and 3, using a numerical depth-averaged two-dimensional k–ε model. The Reynolds number in the vegetation zone is defined by $Re = u_v \phi / \upsilon$, with u_v as the mean flow velocity in that area. According to [10, 11], $u_v = 0.171\ m\ s^{-1}$ for VD = 0.176 m^{-1} while this velocity was not available for VD = 2.739 m^{-1}. The simulated u_v were 0.177 and 0.0043 $m\ s^{-1}$ for VD = 0.176 and 2.739 m^{-1}, giving $Re = 566.4$ and 13.76, respectively. According to the experimental data compiled by [52, Figure 3.15], the drag coefficients fitted agreed reasonably

DOI: 10.1002/fld

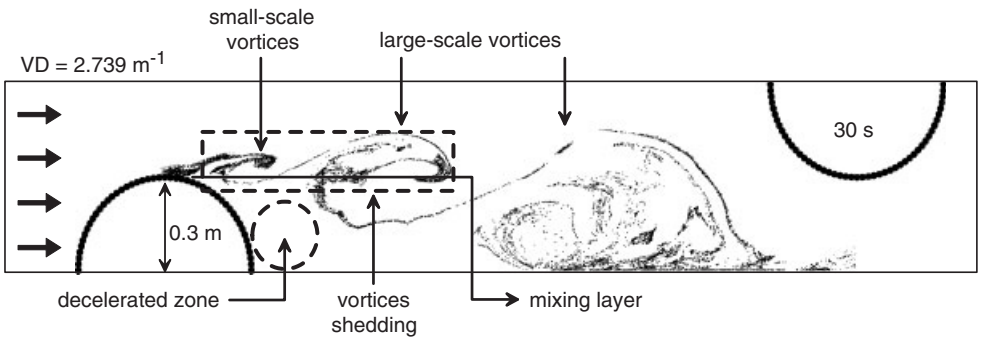

Figure 7. Flow pattern snapshots obtained for $\mathrm{VD} = 2.739\,\mathrm{m}^{-1}$ with the lattice BGK model at 30 s after the particles of a passive tracer were released continuously at the apex of the central vegetation zone in the test section of Figure 4. The flow structures reproduced by the model, such as the mixing layer, decelerated zone and small-scale and large-scale vortices, agree with those described by [11].

well with the ones measured for those Reynolds numbers for a circular cylinder which are ≈ 1.15 and 2.74.

Figure 6 shows the time-averaged surface flow pattern over 100 samples each one taken every 1000 time steps. The simulated influence of the vegetation density was similar to that described by [10]. At $\mathrm{VD} = 0.176\,\mathrm{m}^{-1}$, the flow decelerated in the leeward of the vegetation zones and accelerated in the opposite regions with the time-averaged velocity vectors being straight and parallel. At $\mathrm{VD} = 2.739\,\mathrm{m}^{-1}$, the flow was greatly perturbed by the emergent vegetation. In the same way that [10] reported, the flow was diverted away from the vegetation zone towards the other bank until it encountered the next vegetation zone downstream where it diverted again towards the opposite bank.

Some of the effects of vegetation on turbulent flow structure described by [11] can be seen in Figure 7. The flow patterns were visualized by a large number of particles of a passive tracer released continuously at the apex of the central vegetated zone in the test section of Figure 4. Figure 7 shows the paths followed by the particles at 30 s after they were injected in the computational domain when simulating $\mathrm{VD} = 2.739\,\mathrm{m}^{-1}$. At each time interval Δt, the position $\mathbf{r}$ of a particle was calculated from the velocity $\mathbf{u}'$, derived by applying a bilinear interpolation to the velocity field obtained with the lattice BGK model, according to

$$r_k(t + \Delta t) = r_k(t) + u'_k \Delta t \tag{23}$$

As can be observed in Figure 7, the lattice model reproduced the mixing layer described by [11]. It was created downstream of the vegetation zone associated with small-scale and large-scale vortices, with the axis of rotation normal to the bed. The decelerated zone was placed downstream of the vegetation, and it corresponds to the large near-dead area reported by [11]. The small-scale vortices were located near and downstream of the vegetation zone apex. Their shape was elliptical and they were shed continuously from the vegetated area, being in agreement with the description made by [11]. The large-scale vortices were developed at a distance of about 1 m downstream of the vegetation zone and they had a tendency to fill the entire width of the flume as [11] observed. The rotation direction of both kinds of vortices was towards the vegetated area.

DOI: 10.1002/fld

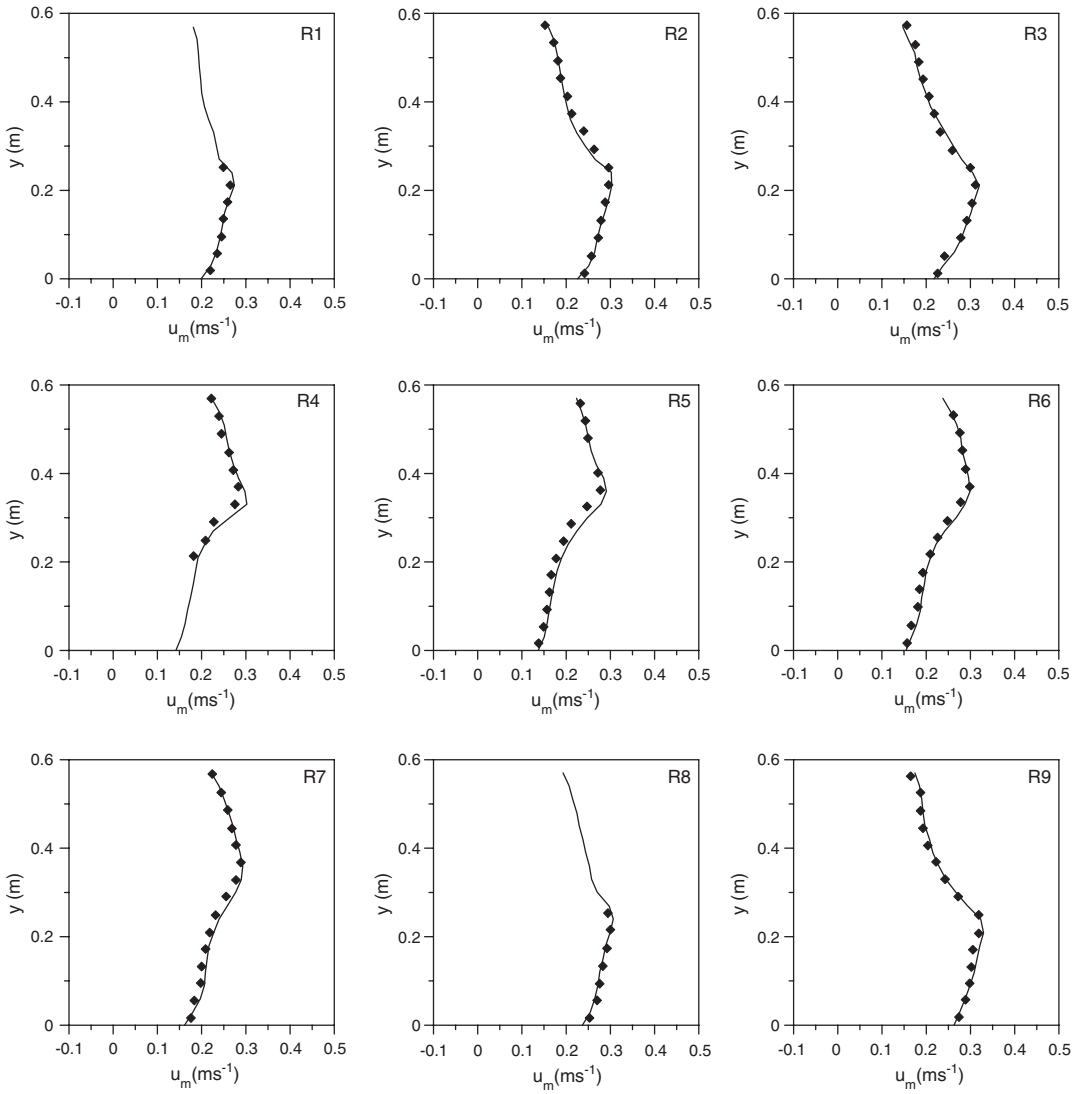

Figure 8. Experimental surface flow velocities (symbols) measured by [10] and reported in [21] and the simulated results (solid lines) using the proposed lattice BGK model in the sections, R_i, marked in Figure 6 when the vegetation density $\mathrm{VD} = 0.176\,\mathrm{m}^{-1}$.

In the test area cross-sections denoted by R_j, $j \in [1, 9]$, in Figure 6, the surface flow velocity was measured by [10] and reported in [21]. Figures 8 and 9 show the experimental data taken by PIV and the results obtained with the proposed lattice BGK model for $\mathrm{VD} = 0.176$ and $2.739\,\mathrm{m}^{-1}$. As shown in those figures, the simulated results were similar to the measurements. The values of the Nash–Sutcliffe efficiency, E, were acceptable as can be seen in Table IV. These results suggest that the lattice BGK model introduced here is particularly appropriate for describing the turbulent structures developed by the effect of the vegetation on open-channel streams.

DOI: 10.1002/fld

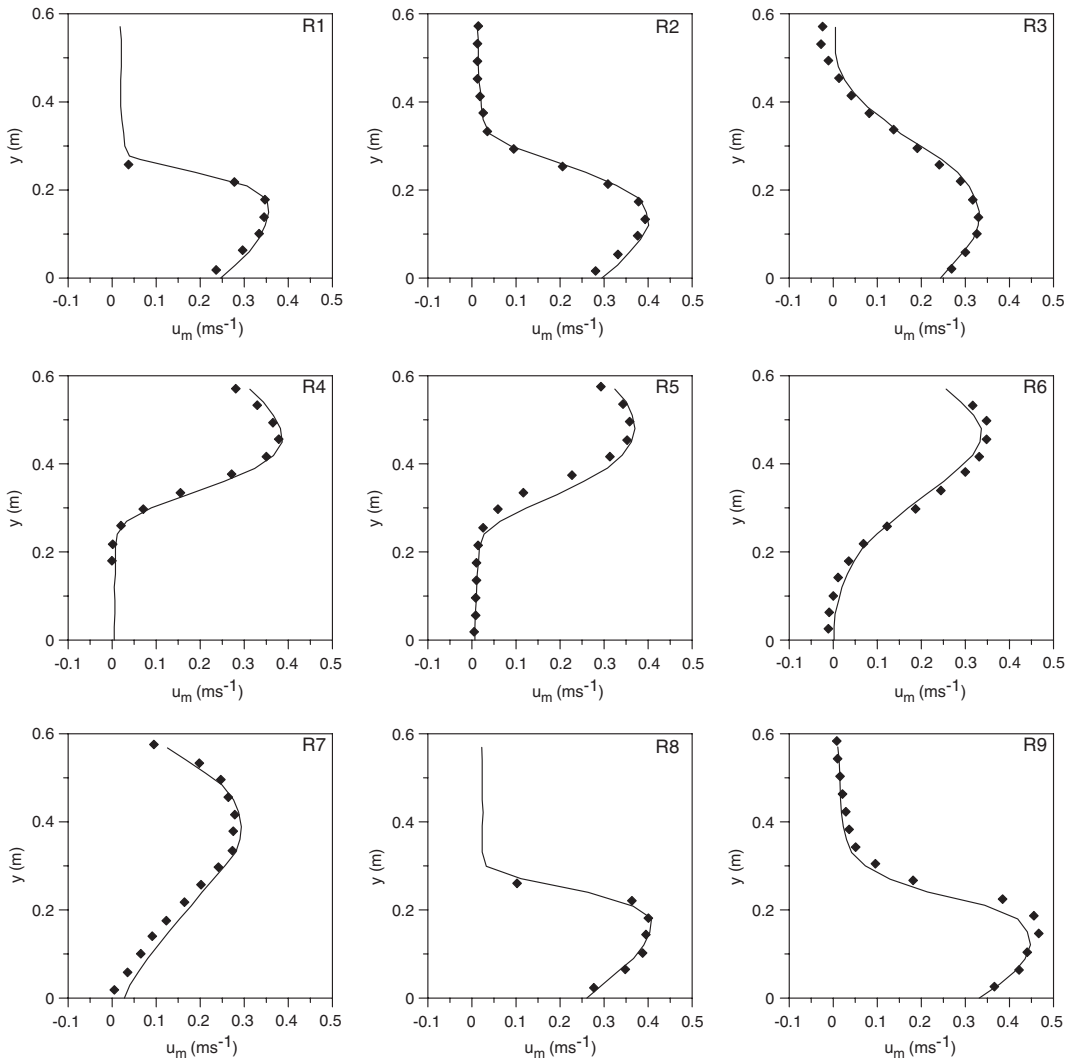

Figure 9. Experimental surface flow velocities (symbols) measured by [10] and reported in [21] and the simulated results (solid lines) using the proposed lattice BGK model in the sections, R_i, marked in Figure 6 when the vegetation density VD = 2.739 m^{-1}.

Table IV. Coefficient of efficiency, E, obtained with the results provided by the lattice BGK model (Figures 8 and 9) for the surface flow velocity in the test cross-sections reported by [10] and marked in Figure 6.

	Section								
VD (m^{-1})	R_1	R_2	R_3	R_4	R_5	R_6	R_7	R_8	R_9
0.176	0.824	0.973	0.979	0.831	0.926	0.981	0.948	0.883	0.984
2.739	0.894	0.992	0.986	0.987	0.955	0.985	0.951	0.913	0.973

DOI: 10.1002/fld

4. CONCLUSIONS

The proposed lattice BGK model has shown itself to be a suitable alternative for describing the water flow in the presence of emergent vegetation arranged in alternate zones along an experimental flume. The simulated time-averaged flow pattern and the surface flow velocities agreed with the experimental results obtained by [10]. The effects of vegetation density on the turbulent flow structure reproduced by the lattice model, including accelerated and decelerated zones, mixing layer and small-scale and large-scale vortices, were similar to those described by [11].

The main features of the numerical model introduced in this work are: (i) The Smagorinsky subgrid scale model for simulating flow turbulence can be straightforwardly included. (ii) A simple semi-slip boundary condition was used for the treatment of solid walls overcoming the drawbacks of applying the standard non-slip boundary condition in turbulent flows at these locations. (iii) The frictional effects of the channel bed and walls, the action of the gravity and the dragging on the vegetation were added in the lattice model as external stresses, permitting us to consider the vegetation density influence on the flow in an easy way. These characteristics make the lattice BGK model a promising tool for being applied to simulate different river restoration techniques.

Some simplifications have been adopted in the proposed model to simulate the vegetation elements, such as assuming them to be cylinders with a shape factor equal to unity. The projected area of the vegetation in the streamwise direction was calculated from these parameters, and then the drag coefficient was calibrated. However, natural vegetation has different features. For this reason, some further work has to be done in collaboration with field and laboratory experiments with the aim of having the possibility of applying the lattice model approach to a wider range of flows in the presence of vegetation, including sediment transport.

ACKNOWLEDGEMENTS

The authors gratefully acknowledge the support of the Spanish Ministry of Education and Research (MEC) Projects AGL2005-05326/AGR and AGL2006-10927-C03-03/AGR. F. J. Jiménez-Hornero wishes to thank the Consejería de Innovación, Ciencia y Empresa, Junta de Andalucía (Ayudas para facilitar el Retorno de Investigadores a Centros de Investigación y Universidades de Andalucía) for their support.

REFERENCES

1. Brookes A, Shields FD (eds). *River Channel Restoration*. Wiley: Chichester, 1996.
2. Simon A, Bennett SJ, Neary VS. Riparian vegetation and fluvial geomorphology: problems and opportunities. In *Riparian Vegetation and Fluvial Geomorphology*, *Water Science Applications Series*, Bennett SJ, Simon A (eds), vol. 8. AGU: Washington, 2004; 1–10.
3. Nepf HM. Drag, turbulence, and diffusion in flow through emergent vegetation. *Water Resources Research* 1999; **35**:479–489.
4. Nepf HM, Vivoni ER. Flow structure in depth-limited, vegetated flow. *Journal of Geophysics Research* 2000; **105**:28547–28557.
5. Nezu I, Onitsuka K. Turbulent structures in partly vegetated open-channel flows with LDA and PIV measurements. *Journal of Hydraulic Research* 2001; **39**:629–642.
6. López F, García MH. Mean flow and turbulence structure of open-channel flow through non-emergent vegetation. *Journal of Hydraulic Engineering* 2001; **127**:392–402.
7. Wilson CAME, Horritt MS. Measuring the flow resistance of submerged grass. *Hydrological Processes* 2002; **16**:2589–2598.
8. Righetti M, Armanini A. Flow resistance in open channel flows with sparsely distributed bushes. *Journal of Hydrology* 2002; **269**:55–64.

DOI: 10.1002/fld

9. Thompson AM, Wilson BN, Hustrulid T. Instrumentation to measure drag on idealized vegetal elements in overland flow. *Transactions of the ASAE* 2003; **46**:295–302.
10. Bennett SJ, Pirim T, Barkdoll BD. Using simulated emergent vegetation to alter stream flow direction within a straight experimental channel. *Geomorphology* 2002; **44**:115–126.
11. Bennett SJ. Effects of emergent riparian vegetation on spatially averaged and turbulent flow within an experimental channel. In *Riparian Vegetation and Fluvial Geomorphology*, *Water Science Applications Series*, Bennett SJ, Simon A (eds), vol. 8. AGU: Washington, 2004; 29–41.
12. Carollo FG, Ferro V, Termini D. Flow velocity measurements in vegetated channels. *Journal of Hydraulic Engineering* 2002; **128**:664–673.
13. Carollo FG, Ferro V, Termini D. Flow resistance law in channels with flexible submerged vegetation. *Journal of Hydraulic Engineering* 2005; **131**:554–564.
14. Fathi-Maghadam M, Kouwen N. Nonrigid, nonsubmerged, vegetative roughness on floodplains. *Journal of Hydraulic Engineering* 1997; **123**:51–57.
15. Wu FC, Shen HW, Chou YJ. Variation of roughness coefficients for unsubmerged and submerged vegetation. *Journal of Hydraulic Engineering* 1999; **125**:934–942.
16. James CS, Birkhead AL, Jordanova AA, O'Sullivan JJ. Flow resistance of emergent vegetation. *Journal of Hydraulic Research* 2004; **42**:390–398.
17. Lee JK, Roig LC, Jenter HL, Visser HM. Drag coefficients for modeling flow through emergent vegetation in the Florida Everglades. *Ecological Engineering* 2004; **22**:237–248.
18. Armanini A, Righetti M, Grisenti P. Direct measurement of vegetation resistance in prototype scale. *Journal of Hydraulic Research* 2005; **43**:481–487.
19. López F, García M. Open-channel flow through simulated vegetation: suspended sediment transport modelling. *Water Resources Research* 1998; **34**:2341–2352.
20. Tsujimoto T. Fluvial processes in streams with vegetation. *Journal of Hydraulic Research* 1999; **37**:789–803.
21. Wu W, Wang SSY. A depth-averaged two-dimensional numerical model of flow and sediment transport in open channels with vegetation. In *Riparian Vegetation and Fluvial Geomorphology*, *Water Science Applications Series*, Bennett SJ, Simon A (eds), vol. 8. AGU: Washington, 2004; 253–265.
22. Wu W, Shields FD, Bennett SJ, Wang SSY. A depth-averaged two-dimensional model for flow, sediment transport, and bed topography in curved channels with riparian vegetation. *Water Resources Research* 2005; **41**:W03015. DOI: 10.1029/2004WR003730
23. Su XH, Li CW. Large eddy simulation of free surface turbulent flow in partly vegetated open channels. *International Journal for Numerical Methods in Fluids* 2002; **39**:919–937.
24. Choi SU, Kang HS. Reynolds stress modeling of vegetated open-channel flows. *Journal of Hydraulic Research* 2004; **42**:3–11.
25. Defina A, Bixio AC. Mean flow and turbulence in vegetated open channel flow. *Water Resources Research* 2005; **41**:W07006. DOI: 10.1029/2004WR003475
26. Succi S. *The Lattice Boltzmann Equation for Fluid Dynamics and Beyond*. Oxford University Press: Oxford, 2001.
27. Chopard B, Hoekstra A. Computational science of lattice Boltzmann modelling. *Future Generation Computer Systems* 2005; **20**:907–908.
28. Tutar M, Holdo AE. Computational modelling of flow around a circular cylinder in sub-critical flow regime with various turbulence models. *International Journal for Numerical Methods in Fluids* 2001; **35**:763–784.
29. Chen S, Doolen G. Lattice Boltzmann method for fluid flows. *Annual Review of Fluid Mechanics* 1998; **30**: 329–364.
30. Wolf-Gladrow DA. *Lattice-gas Automata and Lattice Boltzmann Models*. Springer: Berlin, 2000.
31. Rothman DH, Zaleski S. *Lattice-gas Cellular Automata. Simple Models of Complex Hydrodynamics.* Cambridge University Press: Cambridge, MA, 1997.
32. Chopard B, Droz M. *Cellular Automata Modeling of Physical Systems*. Cambridge University Press: Cambridge, MA, 1998.
33. Chen S, Wang Z, Shan X, Doolen G. Lattice Boltzmann computational fluid dynamics in three dimensions. *Journal of Statistical Physics* 1992; **68**:379–400.
34. Qian YH, D'Humieres D, Lallemand P. Lattice BGK models for Navier–Stokes equation. *Europhysics Letters* 1992; **17**:479–484.
35. Bathnagar P, Gross EP, Krook MK. A model for collision processes in gases. I. Small amplitude processes in charged and neutral one-component systems. *Physical Review B* 1954; **94**:511–525.

36. Nguyen HP, Chopard B, Stoll S. Hydrodynamic properties of fractal aggregates in 2D using lattice Boltzmann simulation. *Future Generation Computer Systems* 2004; **20**:981–991.
37. Hou S, Sterling J, Chen S, Doolen GD. A lattice subgrid model for high Reynolds number flows. *Fields Institute Communications* 1996; **6**:151–166.
38. Smagorinsky J. General circulation experiments with the primitive equations: I. The basic equations. *Monthly Weather Review* 1963; **91**:99–164.
39. Pope SB. *Turbulent Flows*. Cambridge University Press: Cambridge, MA, 2000.
40. Zhou JG. A lattice Boltzmann model for the shallow water equations with turbulence modelling. *International Journal of Modern Physics C* 2002; **13**:1135–1150.
41. Zhou JG. A lattice Boltzmann model for the shallow water equations. *Computer Methods in Applied Mechanics and Engineering* 2002; **191**:3527–3539.
42. Julien PY. *Erosion and Sedimentation*. Cambridge University Press: Cambridge, MA, 1994.
43. Zhou JG. An elastic-collision scheme for lattice Boltzmann methods. *International Journal of Modern Physics C* 2001; **12**:387–401.
44. Shao Y. *Physics and Modelling of Wind Erosion*. Kluwer Academic Publishers: Dordrecht, 2000.
45. Alonso CV. Transport mechanics of stream-borne logs. In *Riparian Vegetation and Fluvial Geomorphology*, *Water Science Applications Series*, Bennett SJ, Simon A (eds), vol. 8. AGU: Washington, 2004; 59–69.
46. Zhang X, Crawford JW, Bengough AG, Young IM. On boundary conditions in the lattice Boltzmann model for advection and anisotropic dispersion equation. *Advances in Water Resources* 2002; **25**:601–609.
47. Legates DR, McCabe GJ. Evaluating the use of 'goodness-of-fit' measures in hydrologic and hydroclimatic model validation. *Water Resources Research* 1999; **1**:233–241.
48. Chow VT, Maidment DR, Mays LW. *Applied Hydrology*. McGraw-Hill: New York, 1988.
49. Lesieur M, Métais O, Comte P. *Large-eddy Simulations of Turbulence*. Cambridge University Press: Cambridge, MA, 2005.
50. Davidson PA. *Turbulence*: *An Introduction for Scientist and Engineers*. Oxford University Press: New York, 2004.
51. Chow VT. *Open-channel Hydraulics*. McGraw-Hill: New York, 1959.
52. Tritton DJ. *Physical Fluid Dynamics*. Oxford University Press: Oxford, 1988.

DOI: 10.1002/fld